

# Complexity Project: The Oslo Model

CID: 01490427

22th February, 2021

**Abstract:** In this project, we computationally investigated the Oslo model: a system which self-organises to a non-equilibrium steady state. This dynamical system was found to display self-organised criticality (SOC). We explored the response of the system to an external perturbation, finding that it could produce events of all sizes distributed according to a power law. We studied the scaling of the height and cross-over time of the system with system size, finding:  $t_c \propto L^2$  and  $h \propto L$  to leading order. The scaling of the standard deviation on the average height and slope was also obtained:  $\sigma_h \propto L^{0.245}$  and  $\sigma_{\langle z \rangle} \propto L^{-0.753}$ . We successfully proposed a scaling ansatz for the behaviour of the height and avalanche probability of the system. We found that this scaling function acted as a blue-print to systems of all sizes, revealing universal behaviour. Finally, we also empirically obtained estimations for two critical exponents:  $\hat{D} = 2.212 \pm 0.002$  and  $\hat{\tau}_s = 1.548 \pm 0.001$ , and studied the effects of corrections to scaling on these estimations.

Structure of the report: in Section 1 and 2 we will introduce the topic and the general characteristics of the Oslo model. Section 3 will study the height of the pile, its time evolution and probability distribution. Finally, Section 4 will explore the avalanche size probability, suggesting a finite-size scaling ansatz and a method for estimating the two critical exponents.

**Word count:**  $\sim 2100$

# 1 Introduction

Multiple systems in Nature consist of a large number of self-interacting components which, in addition to this internal energy or information exchange, can also be driven by an external force. Examples of this are: a collection of electrons under the influence of an external magnetic field, any ecosystem found in Nature, or the stock-market and its community of traders and dealers [1]. Complexity Science is a multidisciplinary field that, among other themes, studies how these different systems may produce a typical common behaviour.

In this project, we explored a set of systems which self-organise to a non-equilibrium steady state. One example of such a system can be illustrated through the sandpile metaphor. Consider a finite table top where we slowly drop grains of sand at random positions. The pile will at first appear flat, until we add enough grains for the first avalanches to be produced. The system will eventually reach a non-equilibrium steady state where the average influx of grains (and energy) will equal the average outflux. The sandpile has ‘self-organised’ into a steady state without the need to tune any control parameters: it is an inherent property of the system. This state is called the ‘attractor’ of the dynamics. The avalanche size is non-linear and it is distributed according to a power law, i.e. with no apparent characteristic scale [1]. Due to this lack of internal scale, the system is referred to as critical [2].

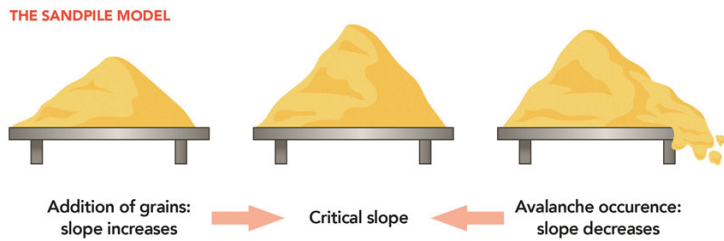


Figure 1: The sandpile model displays self-organised criticality: (if driven slowly) the pile organises itself into a critical state, where the response of the system is non-linear (can span several orders of magnitude). Diagram obtained from [3].

A simple model for this sandpile system was first introduced by Per Bak, Chao Tang and Kurt Wiesenfeld in a paper in 1987 [4]. It consists of a one-dimensional finite system divided into  $L$  sites. Each of the sites is associated with a value that corresponds to the height of the pile at that position. We can work out the slope at each position,  $z_i$ , by obtaining the height difference between consecutive sites. The sites whose slope is larger than a fixed and constant threshold slope,  $z^{th}$ , will relax and the grain will ‘topple’, changing the value of the neighbouring sites’ height and slopes.

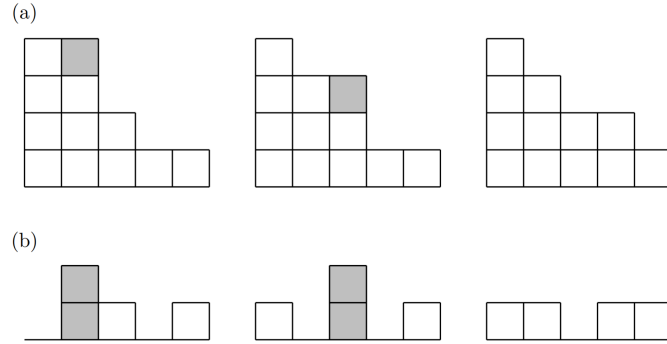


Figure 2: A realisation of an avalanche of size 2 in the one-dimensional BTW model on a system of size  $L = 5$ . A grain is added at site  $i = 2$ . Because  $z_{i=2} > z_{i=2}^{th}$ , an avalanche is initiated.

a) Depict the variations on the heights, while b) presents the relaxation of slopes. Diagram obtained from [2].

Once all the sites have relaxed, (i.e.  $z_i < z_i^{th} \forall i$ ) we have reached a stable configuration. We denote the set of all stable configurations as  $\mathcal{S}$ . This can be divided into a subset of transient configurations,  $\mathcal{T}$ , and a set of recurrent configurations,  $\mathcal{R}$ . The former represents those configurations which can only be encountered once, whereas the configurations in  $\mathcal{R}$  appear indefinitely if the system is driven indefinitely: these are the attractor of the dynamics. The first recurrent configuration will be observed after the 'cross-over' time,  $t_c$ , is reached. This is the number of grains in the system (or time) before an added grain induces a grain to leave the system for the first time.

Although the BTW model is successful at portraying some of the basic features of self-organised criticality (SOC) it is too simple for representing other more sophisticated systems. This rudimentary model does not allow for any temporal or spatial fluctuations: there is one unique recurrent configuration. For this reason, we employ the Oslo model [2] which accounts for two different  $z^{th}$  values. Every time a site relaxes, we reset its slope threshold value,  $z^{th} \in \{1, 2\}$ , where both possibilities have equal probability. This threshold variability portrays the angular degree of freedom observed in systems such as a rice pile, studied by Frette et al in 1996 at the University of Oslo.

The aim of this project was to build an algorithm for the Oslo model and investigate the emergence of SOC and universality. For this purpose we studied the following parameters and their properties: the height of the pile (Section 3) and the avalanche size (Section 4).

## 2 Implementation of the Oslo model

We implemented the Oslo algorithm [2] which was be used throughout the rest of the project. Every time a site relaxes, the threshold is reset by choosing a new value from the distribution:

$$z_i^{th} = \begin{cases} 1 & \text{with probability } p \\ 2 & \text{with probability } 1 - p, \end{cases} \quad (1)$$

where  $p = 0.5$ .

To confirm the successful implementation of algorithm we carried out three different tests following. The results of the tests are summarised in Table 1.

- **Test 1:** Average height post steady state,  $\langle h \rangle$ .

As suggested by the Complexity Project Notes [2], for  $p = 1/2$  the average pile height after the steady state has been reached should average to certain values.

- **Test 2:** Average avalanche size post steady state,  $\langle s \rangle$ .

For  $p = 1/2$ , after the steady state has been reached, the average avalanche size should average to the system size  $\langle s \rangle = L$ .

- **Test 3:** Crossover time  $t_c$  for  $p = 0/1$ .

We know that  $t_c(p = 1) = \frac{1}{2}L(L + 1)$  and  $t_c(p = 0) = L(L + 1)$ . Additionally, for  $p = 0/1 \rightarrow s = L$ .

	$L = 16$	$L = 32$	$L = 64$	$L = 128$
Task 1:				
theory: $\langle h \rangle$	26.5	53.9	-	-
empirical: $\langle h \rangle$	$26.53 \pm 1.14$	$53.88 \pm 1.34$	-	-
Task 2:				
$\langle s \rangle$	$16.00 \pm 45.86$	$32.00 \pm 138.56$	$63.99 \pm 417.76$	$127.92 \pm 1272.72$
Task 3:				
$p = 1/0 : t_c$	136 / 272 $\pm 0.0$	528 / 1056 $\pm 0.0$	2080 / 4160 $\pm 0.0$	8256 / 16512 $\pm 0.0$
$p = 1/0 : s$	16 / 16 $\pm 0.0$	32 / 32 $\pm 0.0$	64 / 64 $\pm 0.0$	128 / 128 $\pm 0.0$
$p = 1/0 : h$	16 / 32 $\pm 0.0$	32 / 64 $\pm 0.0$	64 / 128 $\pm 0.0$	128 / 256 $\pm 0.0$

Table 1: Summary of the results for all tests using the same Oslo algorithm. Note that tasks 1 and 2 had  $p=1/2$  whereas task 3 involved the tuning of the probability to 0 and 1 (left result is for  $p = 1$  and right result for  $p = 0$ ). As a side check, we also noticed that the height of the pile for  $p = 0.5$  was somewhere in between the extremes (i.e.  $p = 0/1$ ). The standard deviation on the average avalanche is remarkably large, caused by the highly non-linear response of the system ( $s$  spans several orders of magnitude). Overall, the values obtained in all tests are within reasonable agreement with the expectation, implying success in the implementation of the model.

### 3 Height of the pile, $h(t; L)$ .

In this section we explored the time evolution of the height of the pile for different system sizes  $L$ , and other statistics associated with them. We investigated how the average height of the pile and the cross-over time scale with  $L$ , and employed this knowledge to produce a data collapse of the height evolution, which allowed us to study scale invariance and universality. Finally, we explored the height probability function  $P(h; L)$ .

#### 3.1 Time evolution of the height for different sizes.

We plot the time evolution of 8 different system sizes ( $L \in \{4, 8, 16, 32, 64, 128, 256, 512\}$ ).

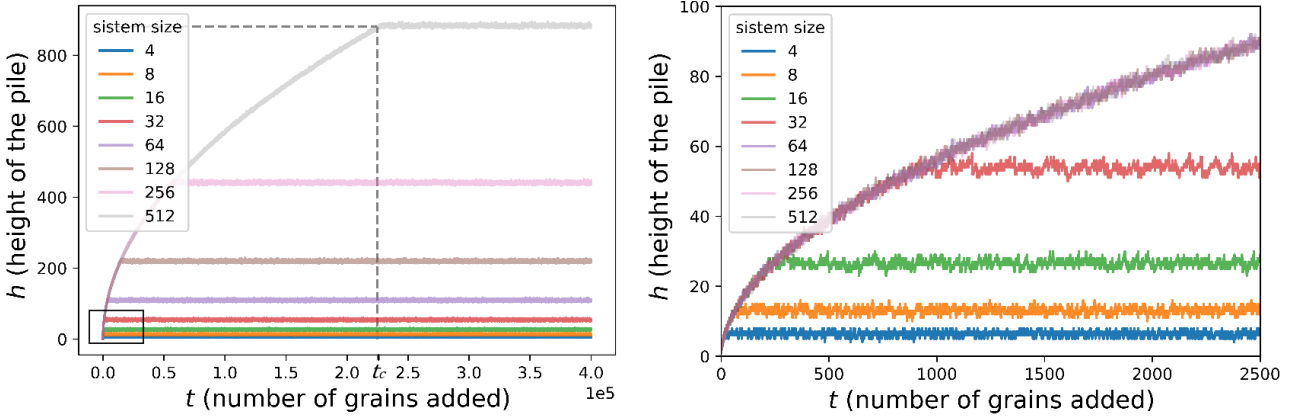


Figure 3: Left: evolution of  $h(t; L)$  for different system sizes. Right: zoomed in to observe height fluctuations. The cross-over time  $t_c$  is labelled for the largest system size on the left plot. Remarkably, all the systems share the same scaling function (a power law) for  $0 < t < t_c$ : the scaling region. This is a property of scale invariance.

As expected, in Figure 3 we can see that after the attractor of the dynamics (the steady state) is reached, the values of the heights oscillate around a mean height. This is a result of the multiple recurrent configurations available. As discussed in the Introduction, if the system was run infinitely many times, all the recurrent configurations will be revisited. This is not the case with the transient configurations, which are only seen once. We also note that when  $\mathcal{R}$  is reached, the number of grains added to the system equals those leaving the system (i.e. in terms of energy  $\langle E_{in} \rangle = \langle E_{out} \rangle$ ), causing the height to oscillate about a value  $\langle h \rangle$ . We will later also investigate in more detail the scaling of the spread of these height oscillations,  $\sigma_h$ . However, qualitatively, we observe an increase in the deviation about  $\langle h \rangle$  with increasing system size.

### 3.1.1 Steady state height scaling: theoretical expectation.

Ignoring corrections to scaling, which will be studied in Subsection 3.4, we devise a theoretical argument to show the scaling of  $h$  with  $L$  in the steady state. Firstly, we can express the height of the pile at any given time  $t$  as the sum of the slopes, such that:

$$h(t; L) = \sum_{i=1}^L z_i(t). \quad (2)$$

Employing this expression, we simply obtain:

$$h(t; L) = \left( \frac{1}{L} \sum_{i=1}^L z_i(t) \right) L = \langle z \rangle L. \quad (3)$$

If we assume that  $\langle z \rangle$  are independent of the system size <sup>1</sup> for  $L \gg 1$  when  $t \gg t_c$ , then clearly  $h \propto L$  to leading order.

---

<sup>1</sup>We know  $\langle z \rangle$  is  $L$ -independent to leading order because  $\langle z \rangle$  is bounded between 1 ( $p=1$ ) and 2 ( $p=1$ ). For  $L \rightarrow \infty$  it will indeed be constant. However, we expect it to show corrections to scaling for finite  $L$ .

## 3.2 Cross-over time $t_c$ .

### 3.2.1 Theoretical expectation.

The cross-over time  $t_c$  is defined as the number of grains in the system *before* an added grain induces a grain to leave the system for the first time. Mathematically that is:

$$t_c = \sum_{i=1}^L z_i \cdot i, \quad (4)$$

where  $z_i$  are the local slopes in the system before an added grain induces a flow out of the system for the first time. The above expression can be easily manipulated to show:

$$t_c = \langle z \rangle \sum_{i=1}^L i = \langle z \rangle \frac{L(L+1)}{2} = \frac{\langle z \rangle}{2} L^2 \left(1 + \frac{1}{L}\right). \quad (5)$$

In the derivation, we have once again used the fact that the average slope is independent of system size. The term  $(1 + \frac{1}{L})$  contains the corrections to scaling. Therefore  $t_c \propto L^2$  is true to leading order.

We can also get an intuitive understanding of the scaling of  $t_c$  by approximating it to be the area,  $A$ , of the triangle that the pile forms. This yields

$$t_c \approx A = \frac{1}{2} L \cdot h \propto L^2, \quad (6)$$

where, in the last step, we have used the result that  $h \propto L$  from Subsection 3.1.1. In the same fashion as Equation 5 the result is only valid for  $L \gg 1$ .

### 3.2.2 Empirical measurements.

To accurately study the scaling of  $t_c$  with  $L$ , we took its average,  $\langle t_c \rangle$ , of over 20 different realisations of the same system. We expect  $t_c$  to show corrections to scaling for the smaller system sizes, therefore, we only considered the larger systems ( $L \geq 64$ ) to produce the fit of the graph.

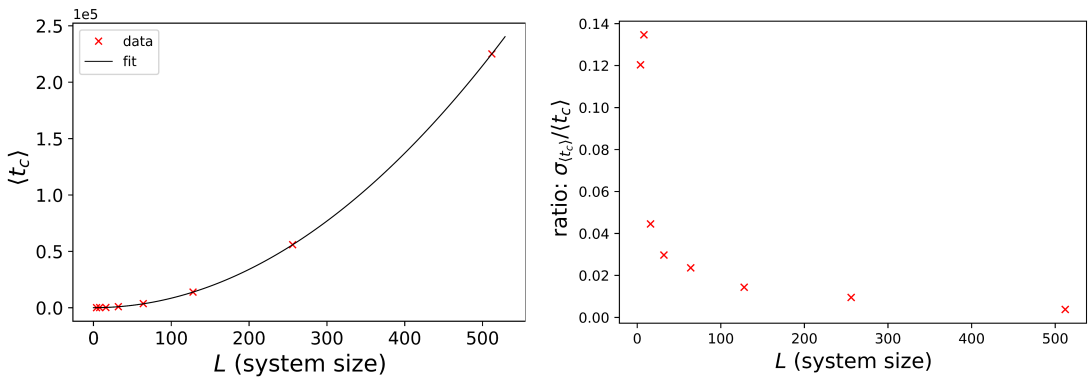


Figure 4: Left: data and fit for average cross-over time  $\langle t_c \rangle$  plotted against different system sizes. Right: ratio of the standard deviation  $\sigma_{\langle t_c \rangle}$  and  $\langle t_c \rangle$ .

For the fit, we only used  $L \geq 64$ , for which we obtain the exponent of the power law of  $\langle t_c \rangle$  to be  $2.01 \pm 0.03$ . The results corroborate the idea that  $t_c \propto L^2$ .

### 3.3 Data collapse: pile height scaling function.

Using our knowledge on the  $L$ -dependence of  $h$  and  $t_c$  (namely:  $h \propto L^2$  and  $t_c \propto L^2$ ), we propose a scaling ansatz to convey the behaviour of the height of the pile:

$$\tilde{h}(t; L) = L^1 \mathcal{F}\left(\frac{t}{L^2}\right), \quad (7)$$

where  $\mathcal{F}$  is a scaling function whose form we aim to identify.

We produced a data collapse for the plot in Figure 3 (normal height evolution) by plotting:

$$\frac{\tilde{h}}{L} \text{ vs } \frac{t}{L^2}. \quad (8)$$

This will reveal the form of the scaling function  $\mathcal{F}$ .

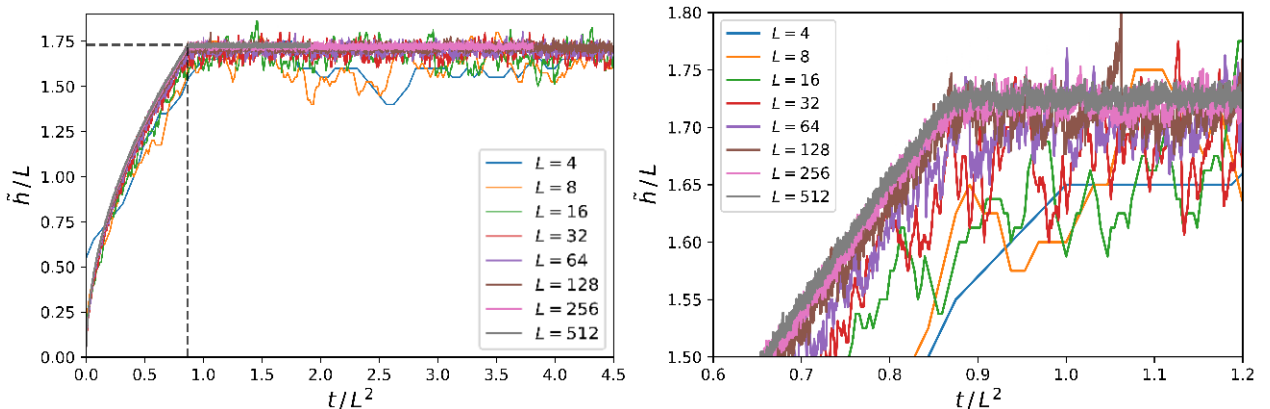


Figure 5: Left: data collapse (trimmed at  $x=4.5$ ), the turning point is signalled with a grey dashed line: ( $\approx \frac{\langle z \rangle}{2}$ ) (0.868), ( $\approx \langle z \rangle$ ) (1.735)). Right: zoomed to transition section of interest.

We observe that the smaller systems do not collapse as successfully into the scaling function. We understand this is due to the corrections to scaling we have discussed in the previous sections.

Note that the data for  $h$  was smoothed by taking the average of 10 realisations for each system, and this was denoted  $\tilde{h}$ .

In Figure 7 we notice two distinct regimes, where the scaling function changes behaviour abruptly. In the regime where  $\frac{t}{L^2} \gg 1$ , for  $L \gg 1$  the function is constant, whereas in the  $\frac{t}{L^2} \ll 1$  it is scale invariant and therefore behaves like a power law. This yields:

$$\frac{h}{L} = \mathcal{F}\left(x = \frac{t}{L^2}\right) = \begin{cases} a_o & \text{for } x \gg 1 \\ c x^\beta & \text{for } x \ll 1 \end{cases} \quad (9)$$

where  $a_o$  and  $c$  are constants, and  $\beta$  is the power law exponent to be determined. We recall from Figure 3 that for  $t \ll L^2$  the evolution of the height of the pile has no knowledge of the system size, meaning it is independent of it. Therefore, we require the scaling function to cancel the  $L$  term in the expression for  $h$ . This is only possible if  $\beta = 1/2$ . This then yields:

$$\tilde{h}(t; L) \propto \begin{cases} L & \text{for } x \gg 1 \\ \sqrt{t} & \text{for } x \ll 1. \end{cases} \quad (10)$$

### 3.4 Corrections to scaling in $\langle h(t; L) \rangle_t$ .

For this section we considered the average height after the system has reached the attractor of the dynamics, namely:

$$\langle h(t; L) \rangle_t = \frac{1}{T} \sum_{t=t_0+1}^{t_0+T} h(t; L) \quad \text{for} \quad t_0 > t_c(L). \quad (11)$$

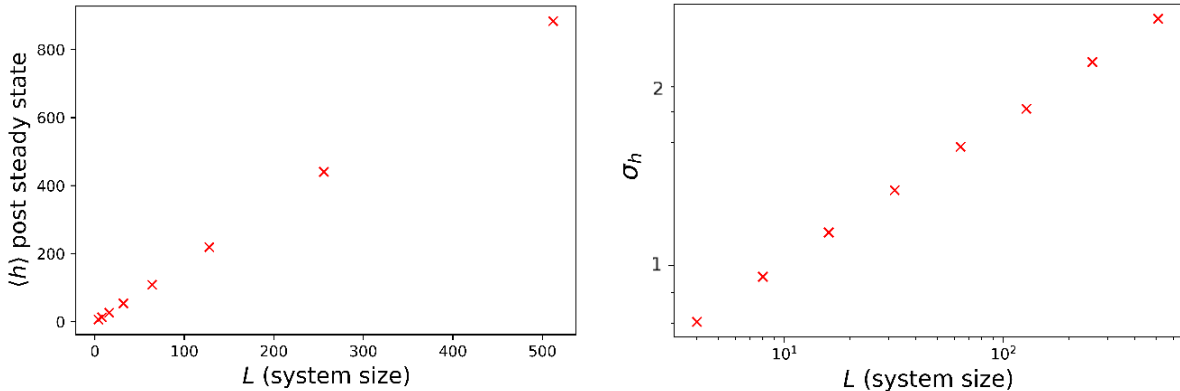


Figure 6: Left: average height in the set recurrent configurations. Right: standard deviation of  $\langle h \rangle$  (log-log plotted). We plotted them separately for clarity, since  $\sigma_h \ll \langle h \rangle$ .

The left plot only reveals the leading order dependency of  $h$  on  $L$ , namely  $h \propto L$  as expected from theory. On the other hand  $\sigma_h$  scales as a power law, that we will investigate in the following section.

We assume the following form for the corrections to scaling:

$$\langle h(t; L) \rangle = a_o L (1 - a_1 L^{-\omega_1} + a_2 L^{-\omega_2} \dots), \quad (12)$$

where  $\omega_i > 0$  and  $a_i$  are constants. We note that, for  $L = \infty$ ,  $a_o$  would be the average slope for this system.

Utilising Equation 12 and neglecting the terms with  $i > 1$  we obtain an estimation for its parameters, presented below in Table 2.

$\hat{a}_o$	$\hat{a}_1$	$\hat{\omega}_1$
$1.734 \pm 0.013$	$0.230 \pm 0.292$	$0.603 \pm 0.396$

Table 2: Estimations obtained for the parameters in Equation 12 by employing a simple curve fitting method.

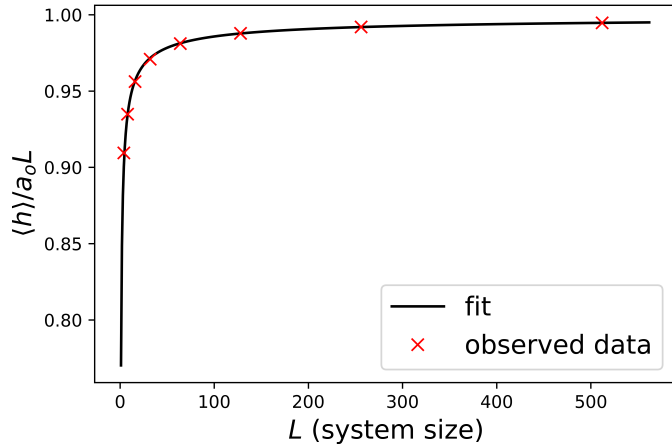


Figure 7: Empirical and fitted data for  $\langle h \rangle$  revealing corrections to scaling caused by the finite size nature of our system. For the fit we have used the parameters estimated in Table 2.

### 3.5 Standard deviation of $\langle h(t; L) \rangle_t$ and $\langle z \rangle_t$ .

As observed in Figure 6, the standard deviation of the height,  $\sigma_h$  scales as a power law with  $L$ . This implies:

$$\sigma_h \propto cL^\gamma, \quad (13)$$

where  $\gamma$  is the exponent to be determined. This is, once again, done by fitting a power law to our data, obtaining the estimated parameters presented in Figure 3.

$\hat{c}$	$\hat{\gamma}$
$0.566 \pm 0.006$	$0.246 \pm 0.002$

Table 3: Estimations obtained for the parameters in Equation 13.

We also wish to investigate whether  $\sigma_h$  contains any signs of corrections to scaling. This was easily done by plotting  $\sigma_h/cL^\gamma$ .

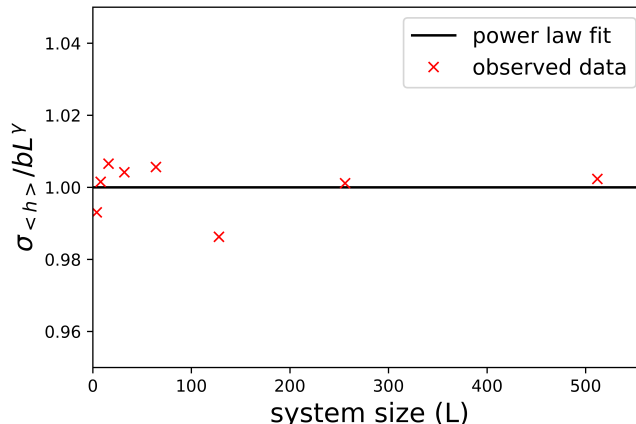


Figure 8: Plot reveals no apparent signs of corrections to scaling, since all values oscillate about the expected value of 1. This means that applying Equation 13 is appropriate.

This now enables us to determine the standard deviation on the mean slope  $\langle z \rangle$ , such that:

$$\sigma_z = \frac{\sigma_h}{L} \propto L^{\gamma-1} \propto L^{-0.753}. \quad (14)$$

This clearly implies that  $\sigma_z \rightarrow 0$  as  $L \rightarrow \infty$ .

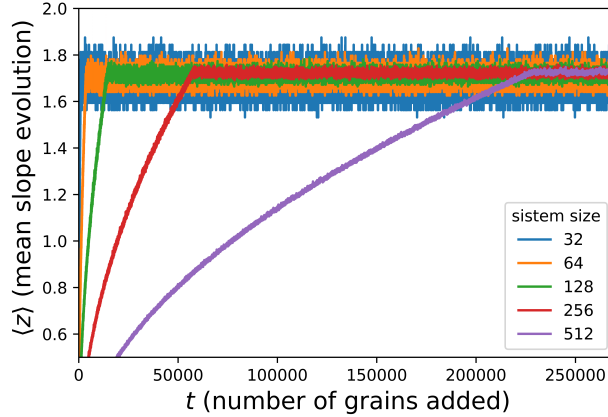


Figure 9: Plot of the mean slope,  $\langle z \rangle$ , evolution with time (i.e. as grains are added to the system) for different system sizes. Note that this is a detail zoomed version of the full graph. The plot corroborates our derivation in Equation 14:  $\sigma_h$  decreases with system size. However, note that the mean slope will differ for each system size: it will only truly equal  $a_o$  for an infinite system.

For the infinite system, we expect  $\langle z \rangle$  to be the true value of  $a_o$  because there would be no finite size effects and so:

$$\langle h \rangle = a_o L = \langle z \rangle L \rightarrow \langle z \rangle = a_o (\approx 1.735) \quad \text{for } L = \infty \quad (15)$$

### 3.6 Height probability distribution, $P(h; L)$

We define the height probability distribution as:

$$P(h; L) = \frac{\text{no. of observed configurations with height } h \text{ in pile of size } L}{\text{total no. of observed configurations}}. \quad (16)$$

If one naively assumed that  $z_i$  are independent, identically distributed random variables with finite variance we could apply the Central Limit Theorem (CLT) [5]. This states that  $P(h; L)$  is well approximated by a normal (Gaussian) distribution such that:

$$P(h; L) = \frac{1}{\sqrt{2\pi}\sigma_h} \exp \left[ -\frac{1}{2} \left( \frac{h - \langle h \rangle}{\sigma_h} \right)^2 \right]. \quad (17)$$

The CLT assumptions we have made also predict that  $\sigma_h \propto \sqrt{L}$ . However, from our empirical results shown previously in Table 3 we know this to be untrue:  $\sigma_h \propto L^{0.25}$ . We will observe the implications of the incorrect implementation of the CLT later.

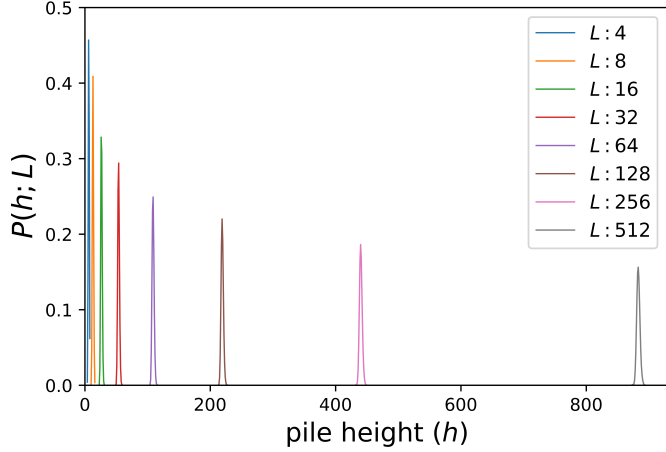


Figure 10: Height probability distribution for different system sizes. At a first glance, the distributions appear Gaussian. We observe the width of the functions increase (as  $\sigma_h$ ) with system size  $L$ , whereas  $P_{max}$  decreases as  $1/\sigma_h$ . This also ensures the distributions are correctly normalised.

We now wish to study the data by producing a data collapse to a Gaussian distribution with  $\mu = 0$  and  $\sigma = 1$ , which we denote with the letter  $\mathcal{G}$ . This implies:

$$\sigma_h P(h; L) = \mathcal{G}(y) = \frac{1}{\sqrt{2\pi}} \exp\left(-\frac{1}{2}y^2\right) \quad \text{where} \quad y = \frac{h - \langle h \rangle}{\sigma_h}. \quad (18)$$

And so, to see the data collapse, we are required to plot  $\sigma_h P(h; L)$  vs  $\frac{h - \langle h \rangle}{\sigma_h}$ .

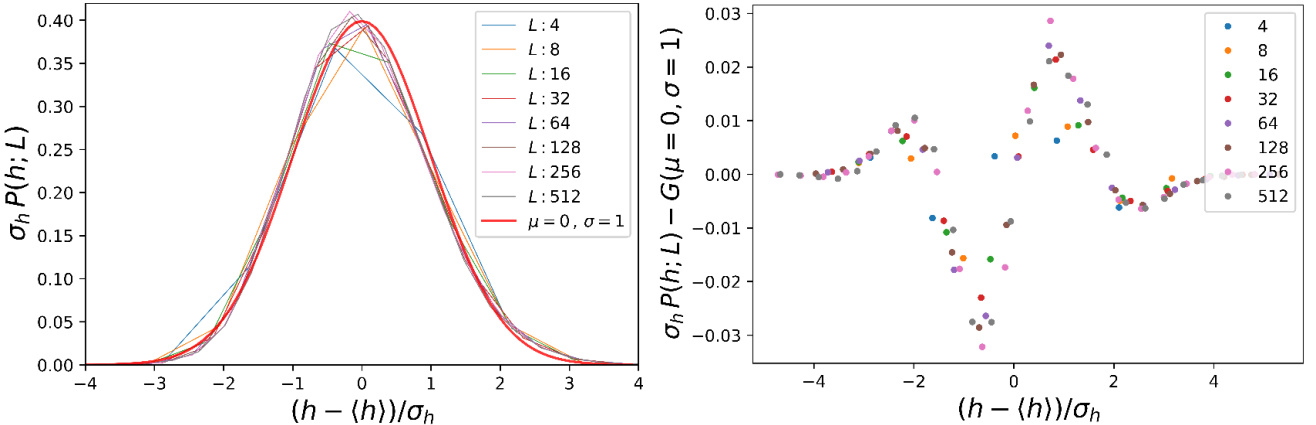


Figure 11: Left: collapsed height probability distributions and expected Gaussian of  $\mu = 0$ ,  $\sigma = 1$ . Right: residues of the observed data from the expected data.

As expected from our previous discussion, the observed collapsed data does not accurately match the theoretical expected Gaussian. From the right plot we see that this inaccuracy appears to be  $L$ -independent, i.e. the plot doesn't get more Gaussian with increasing system size. In addition, the residues seem to trace out a characteristic shape, they are not normally distributed, meaning that the lack of Gaussianity is not accidental.

Our findings can attributed to the fact that the slopes of the system,  $z_i$ , are not independent. Due to the nature of the Oslo model, the slopes of neighbouring sites are correlated (the correlation length does not go to zero for  $L = \infty$ , meaning that the slope dependency

will be relevant for all system sizes). One way to see the correlation of sites is by noticing that site  $i$  will not topple unless site  $i - 1$  has. This means that the CLT does not apply. One way to test this argument is to shuffle the slopes across time for all sites, which would make the slopes independent and therefore the CLT will be appropriate. In this case, we would expect  $\sigma_h \propto \sqrt{L}$ .

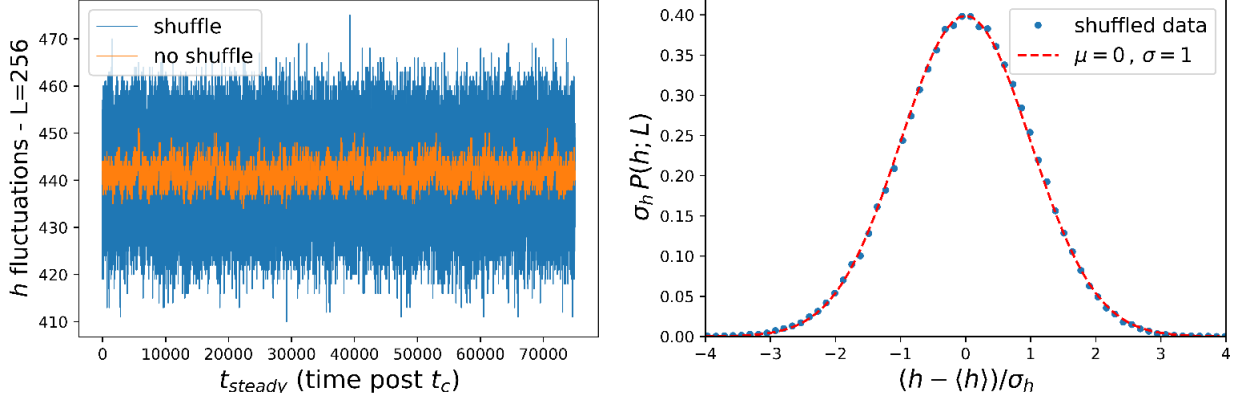


Figure 12: Left: height fluctuations obtained from shuffled slopes vs original slopes. Right: collapsed shuffled slope height probability distribution for  $L = 256$  and expected Gaussian of  $\mu = 0, \sigma = 1$ . We found the  $\sigma_h$  from the shuffled slopes to scale as  $\sigma_h \propto \sqrt{L}$ , as expected from the CLT. Additionally, the collapsed data fits the Gaussian more accurately than those in Figure 11, corroborating our conclusion that it is the dependency of the  $z_i$  that causes the deviation from the Gaussian in the original Oslo model.

## 4 Avalanche size probability, $P(s; L)$ .

In the Oslo model, the avalanche sizes span many orders of magnitude, meaning the response of the system is highly non-linear.

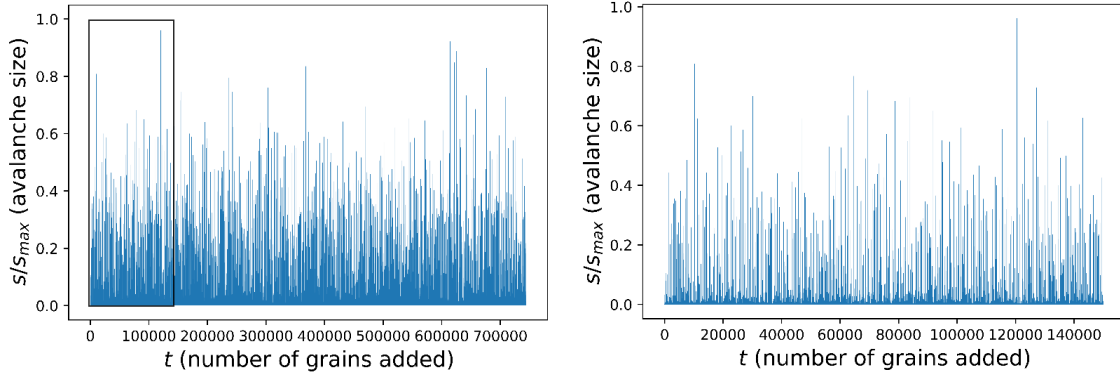


Figure 13: Left: normalised avalanche sizes for  $L = 256$  (this is not the complete data set). Right: zoomed in section of the left graph.

There is a large variability in avalanche sizes with the frequency of avalanches decaying with size. The largest avalanche recorded was 235579. As expected  $\langle s \rangle = L$ . The avalanche sizes behave in a fractal (self-similar) manner: the scale at which we observe the plot does not affect its observed shape.

We now investigate the avalanche-size probability and associated moments.

We estimate an underlying avalanche size probability  $P(s; L)$  by sampling a finite set of

$N$  avalanches  $\{s_1, s_2, \dots, s_N\}$ . We define:

$$P_N(s; L) = \frac{\text{no. of avalanches of size } s_i = s}{N}. \quad (19)$$

Using this expression, the underlying avalanche size probability  $P(s; L)$  is defined as:

$$P(s; L) = \lim_{N \rightarrow \infty} P_N(s) \approx P_N(s) \quad \text{for } N \gg 1. \quad (20)$$

#### 4.1 Log binning of $P_N(s; L)$ .

For those systems of large size we would obtain scatter data for  $P_N(s; L)$  if our set of avalanches ( $N$ ) is not large enough, due to the insufficient statistics for the larger avalanches, which are very rare. This scatter data does, however, contain information about the underlying probability profile,  $P(s)$ , which we can extract using a method called data binning 2. This consists of dividing the avalanche sizes into exponentially increasing bins and then we count the number of avalanche within that bin. We then divide by the number of avalanches in total that we have measured and the width of the bin. We can tune the scale parameter controlling the growth of bin sizes,  $a$ . We will denote this log binned data as  $\tilde{P}_N(s; L)$ . Our challenge was to run a large number of iterations  $N$  (larger  $N$  required for increasing  $L$ ) and make the bins' scale  $a$  as small as possible, while still producing a smooth curve for  $\tilde{P}_N(s; L)$ .

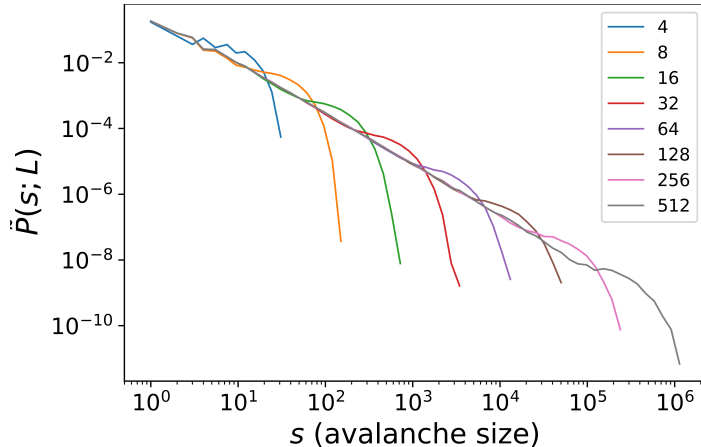


Figure 14: Log-binned  $P_N(s; L)$  for different system sizes, for  $a = 1.25$  and  $N \approx 800,000$ . The plots portray the expected shape: a scaling region ( $1 \ll s \ll s_c$ ) which decays as a power law, followed by a 'bump' at around  $s_c$  (the avalanche size cut-off) which leads to a rapidly decaying region. The scaling region for all system sizes shares the same power law function (scale invariance). We notice that for the smaller system sizes (such as  $L = 4$ ) the scaling region is almost non-existent<sup>2</sup>. There is no typical size of an avalanche except for  $s_c$  (cutoff avalanche size) which increases with  $L$ .

The 'bumps' (located at  $s \sim s_c$ ) observed for the plots in Figure 14 are associated with the system spanning avalanches where grains are dropping out at the right boundary next to  $i = L$ . These avalanches would have been larger in a larger system but are 'truncated' and therefore create an excess probability around  $s_c$ . The bump will disappear for  $L = \infty$ .

---

<sup>2</sup>We will understand this phenomenon when we consider the scaling function for  $P(s; L)$  in the next subsection, and how it is only valid for  $L, s \gg 1$ .

## 4.2 Finite-size scaling ansatz for $P(s; L)$ .

We now propose a simple finite-size scaling ansatz for the avalanche-size probability,  $P(s; L)$ , valid for large avalanches and system sizes:

$$\text{for } L \gg 1 \text{ and } s \gg 1 : \quad P(s; L) \propto s^{-\tau_s} \mathcal{G}(s/s_c), \quad \text{where } s_c = bL^D, \quad (21)$$

where the critical exponent  $D$  is the avalanche dimension, the critical exponent  $\tau_s$  is the avalanche-size exponent and  $b$  is a constant. We have also introduced  $\mathcal{G}(x)$ , the scaling function, whose shape we can predict by examining Figure 14: it must decay sufficiently fast for large avalanche sizes to ensure  $\langle s^k \rangle$  exists  $\forall k$  and, assuming it is well behaved for  $x \ll 1$ , we expect:

$$s^{\tau_s} P(s; L) \propto \mathcal{G}\left(x = \frac{s}{s_c}\right) \propto \begin{cases} \mathcal{G}(0) + \mathcal{G}'(0)x + \frac{1}{2}\mathcal{G}''(0)x^2 + \dots \approx \mathcal{G}(0) & \text{for } x \ll 1 \\ \text{rapid decay} & \text{for } x \gg 1. \end{cases} \quad (22)$$

We note that we require  $L \gg 1$  and  $s \gg 1$  so that we can safely reject the corrections to scaling in  $s_c$  and  $P(s; L)$ , namely:

$$s_c(L) = bL^D(1 + b_1L^{-\nu_1} + b_2L^{-\nu_2} + \dots) \approx bL^D \quad (23)$$

$$P(s) = ms^{-\tau_s}(1 + m_1L^{-\Omega_1} + m_2L^{-\Omega_2} + \dots) \approx ms^{-\tau_s}, \quad (24)$$

for  $\nu_i, \Omega_i > 0$ . Due to these corrections to scaling, we do not expect  $\tilde{P}(s; L)$  to collapse accurately unless  $L, s \gg 1$ .

To produce the data collapse, we must plot:  $s^{\tau_s} P(s; L)$  vs  $s/L^D$ . We can obtain estimations for  $\tau_s$  and  $D$ , and tune them to produce the best collapse:

- $\tau_s$ : we fitted Equation 24 up to first order correction for  $L = 512$  in Figure 14 and estimated the exponential to be  $\hat{\tau}_s = 1.555 \pm 0.006$ . In Figure 15, the factor of  $s^{\tau_s}$  flattens the scaling region, turning it into a constant.
- $D$ : we found a way to relate  $D$  to a parameter we had estimated previously:  $\sigma_h$ .  $L^D$  represents the scaling of the cut-off avalanche size and knowing that  $L^\gamma$  (see Equation 13) is the scaling of the deviation on the mean height (variation in the relation between  $h$  and  $L$ ). Then clearly:  $s_c \propto L^D \propto L^{2+\gamma}$  and so  $D = 2.246 \pm 0.002 \approx 2.25$  (Table 3). In the data collapse, dividing by  $L^D$  will shift the ‘bumps’ to make them align.

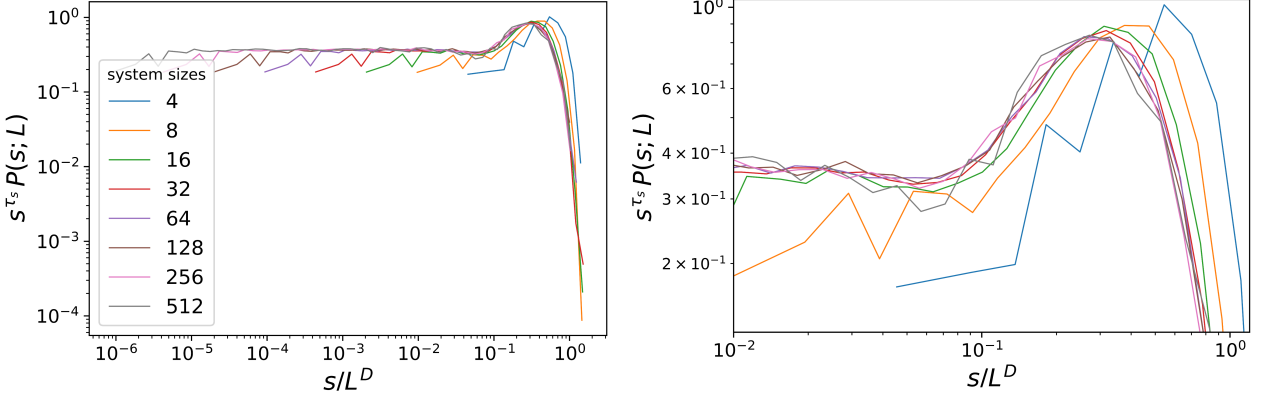


Figure 15: Left: scaling function  $\mathcal{G}$  for avalanche size probability for which  $\tau_s = 1.55, D = 2.246$ . Right: close-up zoom in to 'bump'.

We observe the expected behaviour: constant and rapid decay. On the right plot we can see the effects of the corrections to scaling for the smaller system sizes, for which the scaling ansatz is no longer suitable

### 4.3 Moments of the avalanche size, $\langle s^k \rangle$ .

We define the  $k$ 'th moment of the avalanche size as:

$$\langle s^k \rangle = \lim_{T \rightarrow \infty} \frac{1}{T} \sum_{t=t_0+1}^{t_0+T} s_t^k, \quad (25)$$

where  $s_t$  is the measured avalanche size at time  $t$  and  $t > t_c$ . Assuming the finite size scaling in Equation 21,  $\langle s^k \rangle$  can be conveniently rewritten in terms of system size [2]:

$$\langle s^k \rangle \propto L^{D(1+k-\tau_s)}. \quad (26)$$

We have previously discussed that  $\langle s \rangle \propto L$ , and so for  $k = 1$  we can infer the following scaling relation <sup>3</sup>:

$$\langle s \rangle \propto L \propto L^{D(2-\tau_s)} \rightarrow D(2 - \tau_s) = 1. \quad (27)$$

This relation is consistent with the values of  $D$  and  $\tau_s$  we estimated in the previous section:  $D(2 - \tau_s) = 2.25(2 - 1.55) \approx 1$ .

Recall that the finite size scaling ansatz was only valid for  $L, s \gg 1$ , so we expect to see some corrections to scaling in  $\langle s^k \rangle$ , as presented in Figure 16.

---

<sup>3</sup>Interestingly, this scaling relation is only true for a boundary drive Oslo model. For a bulk driven Oslo model we should study its new scaling between  $\langle s \rangle$  and  $L$ .

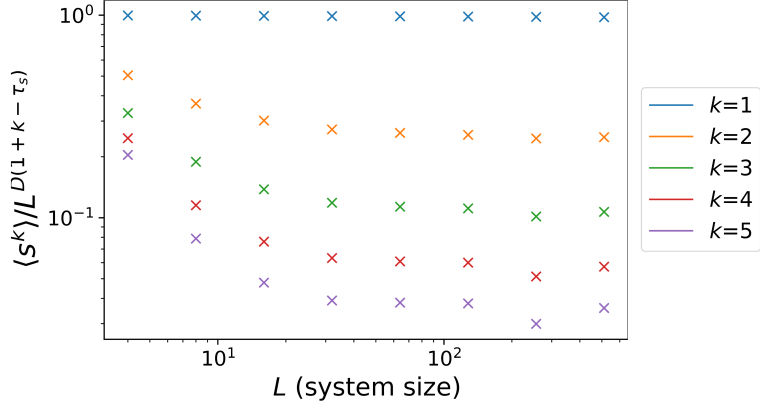


Figure 16:  $k$ 'th moment of avalanche size divided by  $D(1 + k - \tau_s)$  to reveal corrections to scaling. The corrections increase with  $k$  for the smaller  $L$ . Guided by this, we see that a more accurate result will be yielded for  $L \geq 64$ .

Taking the logarithm on both sides of Equation 26:

$$\log(\langle s^k \rangle) = D(1 + k - \tau_s) \log(L) + n_1 = m_k(k) \log(L) + n_1, \quad (28)$$

where  $n$  is a constant. We employed linear regression to obtain the estimates of  $m_k$ .

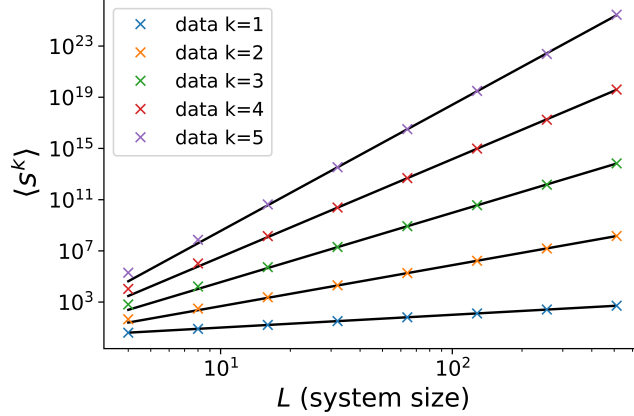


Figure 17: Data and fit (black) for the  $k$ 'th moment of the avalanche size against system size  $L$ . As discussed in Figure 16 only those systems with  $L \geq 64$  were used for the fit. The slopes of the fitted lines are the values of  $m_k(k)$ . The corrections to scaling are noticeable for small  $L$ .

We can now finally estimate  $D$  and  $\tau_s$  by considering  $m_k$  against  $k$ . These will be related as follows:

$$m_k(k) = D(1 + k - \tau_s) = Dk + n_2 \quad \text{where } n_2 = D - D\tau_s. \quad (29)$$

This way, we obtain:  $\tau_s = 1 - nD$ .

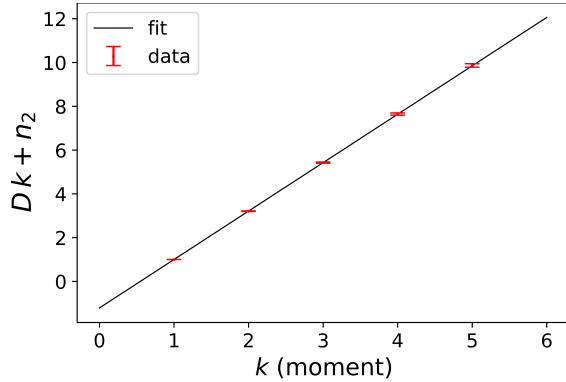


Figure 18: Data and fit for  $m_k$  ( $Dk + n_2$ ) vs  $k$  (moment) only using  $L \geq 64$ . The fit yielded:  $\hat{D} = 2.212 \pm 0.002$  and  $\hat{n}_2 = -1.213 \pm 0.002$ . Errors on the  $m_k$  data values are seen to increase with  $k$ .

As a side test to observe the corrections to scaling we decided to obtain  $\hat{D}$  and  $\hat{\tau}_s$  for different combinations of system sizes. All our results are presented in Table 4.

	$64 \leq L \leq 512$	$4 \leq L \leq 512$	$4 \leq L \leq 64$
$\hat{D}$	$2.212 \pm 0.002$	$2.139 \pm 0.010$	$1.998 \pm 0.020$
$\hat{\tau}_s$	$1.548 \pm 0.001$	$1.533 \pm 0.005$	$1.499 \pm 0.011$

Table 4: Estimations obtained for  $D$  and  $\tau_s$  when considering different sets of system sizes. The first column ( $64 \leq L \leq 512$ ) is obtained from Figure 18. The error on  $\tau_s$  has been obtained through propagation of errors from  $\sigma_{\hat{D}}$  and  $\sigma_{\hat{n}}$ . The effect of the corrections to scaling is clear: the larger system sizes provide a better estimate for  $D$  and  $\tau_s$  with smaller estimated error.

## 5 Conclusions

Given the successful computational implementation of the Oslo model, we were able to explore its major feature: self-organise criticality. One of the most remarkable findings associated with SOC was the verification of the finite-size scaling function for the avalanche size probability, which portrays how different systems originate from the same blue-print. With our computational framework we were also able to show the effect of the corrections to scaling, which were significant in the estimation of the critical exponents.

What I personally found most striking was how such complex behaviour can emerge from simple neighbouring-sites interaction, and then how this complex behaviour can be simplified back by an ansatz that work across all scales.

*The aim of the science self-organized criticality is to yield insight into the fundamental question of why nature is complex, not simple, as the laws of physics imply.*

---

Per Bak

## References

- [1] G. Pruessner, Self-organised Criticality, Cambridge University Press (2012).
- [2] K.Christensen and N.Maloney, *Complexity and Criticality*, Imperial College Press, London, 2005.
- [3] Janina Hesse, Thilo Gross. Self-organized criticality as a fundamental property of neural systems, 2014.
- [4] Bak, P., Tang, C. Wiesenfeld, K., Self-organized criticality: An explanation of 1/f noise, 1987.
- [5] Mark Richards, Statistics of Measurement, Year 2 Lecture Notes, Imperial College London (2019).